





Article

On the Influence of Binder Material in PCBN Cutting Tools for Turning Operations of Inconel 718

Francisco Matos ¹, Tiago E. F. Silva ², Vitor F. C. Sousa ^{2,*}, Francisco Marques ³, Daniel Figueiredo ³,
Francisco J. G. Silva ⁴ and Abílio M. P. de Jesus ^{1,2}

¹ DEMec, Department of Mechanical Engineering, Faculty of Engineering, University of Porto, 4200-465 Porto, Portugal

² INEGI, Institute of Science and Innovation in Mechanical Engineering, University of Porto, 4200-465 Porto, Portugal

³ Palbit, S.A., Product Development Department, 3854-908 Branca, Portugal

⁴ ISEP, School of Engineering, Polytechnic of Porto, 4200-072 Porto, Portugal

* Correspondence: vsousa@inegi.up.pt

Abstract: Inconel 718 is a highly valued material in the aerospace and nuclear industries due to the fact of its exceptional properties. However, the processing of this material is quite difficult, especially through machining processes. Machining this material results in rapid tool wear, even when low material removal rates are considered. In this study, instrumented turning experiments were employed to evaluate the machinability of Inconel 718 alloy using PCBN tools while assessing the usage of two distinct binder phases, TiN and TiC, for those cutting tools. It was found that the tool life was highly sensitive to the cutting speeds but also affected by the workpiece mechanical properties. At lower cutting speeds, notch wear significantly impacted the tool integrity, whereas at higher cutting speeds, flank wear was the primary failure mode of the tool. The flank wear of the tools with TiN-based binder outperformed TiC by almost 30%, presenting a more consistent behavior when machining.

Keywords: Inconel 718; PCBN cutting tools; tool binder material; machinability assessment; tool wear



Citation: Matos, F.; Silva, T.E.F.; Sousa, V.F.C.; Marques, F.; Figueiredo, D.; Silva, F.J.G.; Jesus, A.M.P.d. On the Influence of Binder Material in PCBN Cutting Tools for Turning Operations of Inconel 718. *Metals* **2023**, *13*, 934. <https://doi.org/10.3390/met13050934>

Academic Editor: George A. Pantazopoulos

Received: 13 March 2023

Revised: 17 April 2023

Accepted: 6 May 2023

Published: 11 May 2023



Copyright: © 2023 by the authors. Licensee MDPI, Basel, Switzerland. This article is an open access article distributed under the terms and conditions of the Creative Commons Attribution (CC BY) license (<https://creativecommons.org/licenses/by/4.0/>).

1. Introduction

Nickel superalloys, such as Inconel 718, are well known for their excellent mechanical properties, even at elevated temperatures [1,2]. This makes these superalloys the choice material for applications that are quite aggressive and require high mechanical strength at higher temperatures. For example, these alloys are employed in the making of turbine components that operate at temperatures above 800 °C. In addition to their high mechanical properties, these alloys also exhibit high resistance to corrosion and oxidation phenomena [3], making them suited for a wide variety of industries, such as the defense, food processing, automotive, and aeronautical and aerospace industries, in which more Inconel 718 is used [4,5].

Inconel 718 is also known for being a hard material to process, especially with machining operations, and it is classified as a hard-to-cut metal. This is due to the fact of their high mechanical property values coupled with the fact that this alloy has low thermal conductivity and a tendency to work harden [6]. Furthermore, the metallurgical structure of Inconel 718 has a significant number of hard carbides, namely, TiC and NbC, which causes the material to exhibit highly abrasive behavior while being cut [7]. As such, the main problems encountered when machining Inconel 718 is the short tool life caused by the high abrasive wear, high cutting temperatures [8], and tendency of the metal to adhere to the tools' surface. Moreover, the machining of this material damages the workpiece itself at a microstructural level due to the very high cutting forces generated during the process,

as well as the surface tearing and distortion of the final machined components [9]. This is a problem as most aircraft engine components are obtained via machining.

A wide variety of strategies can be employed to mitigate the problems faced when machining hard-to-cut materials, such as the use of tool coatings or novel tool geometries [10]. Alternative machining strategies are also employed to mitigate problems that arise from machining Inconel 718, such as laser-assisted machining aimed at improving surface quality [11] or even different machining strategies using robotics with cutting force control to improve the surface quality of Inconel components, including turbines [12]. Hard coating offers many advantages, especially by improving the wear resistance of cutting tools [13]. However, there are some machining strategies that can be employed in the machining of these hard-to-cut materials, such as high-speed machining (cutting speeds over 120 m/min). This strategy has shown some potential in the machining of hardened steels [14,15], titanium alloys [16,17], and super alloys [18,19]. By employing this machining strategy, higher material removal rates can be achieved (compared to conventional machining). Nonetheless, employing this strategy using carbide tools (uncoated or coated) causes severe tool wear and coating delamination, primarily due to the high abrasive wear caused by the Inconel 718. As such, some alternative tool materials can be employed, such as cBN (cubic boron nitride) or PCBN (polycrystalline cubic boron nitride), which has excellent chemical inertness, high thermal stability, and very high hardness (being second to diamond) [20]. CBN can better maintain its mechanical strength values when subjected to higher temperatures compared to other conventional tool materials; moreover, due to the fact of its high hardness values, it has excellent abrasion resistance [21]. Regarding its resistance to diffusion phenomena, PCBN can resist interactions with the iron present in Inconel 718 up to temperatures of 1300 °C, both for low and high contents of CBN [22].

PCBN tools can be divided into three categories: low content CBN (50–65%); high content CBN (80–90%); and binderless sintered CBN (no binder) [23]. Several studies have been conducted to determine the most appropriate cutting tools for turning Ni-based alloys at higher cutting speeds. Criado et al. [21] compared the performance of low-content PCBN tools and carbide tools during machining operations of Inconel 718. In this study, it was found that the PCBN tools could handle higher cutting speeds, however, at lower values of depth of cut compared to the uncoated WC cutting tools. However, the authors concluded that even with this parameter's adjustment, the PCBN tools had an increased value for machined volume compared to the WC cutting tools while retaining a very similar level of tool wear. Regarding the machined surface roughness, the best quality was obtained using the PCBN tools, which outperformed the WC cutting tools by up to five times in this regard. Studies such as these highlight the potential of using these PCBN tools, particularly for finish-turning operations of Inconel 718. Dudzinski et al. [19] stated that although carbide tools are suited for machining Inconel 718 at lower cutting speeds (between 20 and 30 m/min), for enhanced productivity, ceramic tools are a more appropriate choice, even when considering that WC tools are less prone to crater wear compared to ceramic cutting tools.

Costes et al. [24] analyzed the influence of CBN content when finishing Inconel 718. The authors found that percentages of CBN content in the range of 45–60% in the cutting tool and used at cutting speeds between 250 m/min and 300 m/min led to the best behavior in terms of the best machined surface quality and least amount of sustained wear. Bushlya et al. [25] compared the performance of coated and uncoated PCBN (50% CBN content) with whisker-reinforced alumina tools in high-speed turning operations of Inconel 718. It was concluded that the tool life was highly sensitive to the variations in the cutting speed. The whisker-reinforced alumina tool life was lower than that of the coated and uncoated PCBN tools. The authors also studied the developed cutting forces during the machining operations, finding that these force values were higher for the whisker-reinforced alumina tools compared to the PCBN cutting tools. However, the cutting forces were slightly higher for the coated PCBN cutting tools.

Still, regarding studies conducted on the use of PCBN tools, Khan et al. [26] reported that a 0.2 mm/rev feed rate and a cutting speed value of 300 m/min offered a good productivity/material removal rate when turning Inconel 718. However, in TiN-coated PCBN inserts, as the cutting speed value increased from 300 m/min to 350 m/min, no significant improvement in the performance of the tool life was noticed. This is due to the rapid oxidation of the coating layer [26,27]. Bushlya et al. [28] also tested TiN-coated PCBN tools, comparing them with uncoated PCBN tools. Again, the coated tools produced higher cutting forces during the turning than those observed for the uncoated PCBN tools. In addition, the coated PCBN tools did not produce the best results in terms of the machined surface quality. Some experimental tests showed that low-content CBN tools with TiN binder correspond to excellent wear resistance because the ceramic binder phase has better chemical stability with respect to nickel [29,30].

Understanding tool wear and the developed wear mechanisms during machining is crucial, especially when optimizing a certain process. Wear generally occurs over time, and this failure is a gradual, cumulative process that affects the tool life [31]. As such, studies evaluating the wear behavior of cutting tools can provide useful information about the optimization of the cutting process. Understanding and predicting the effect of the selected cutting parameters on the tool life and wear behavior are also very important. Cores et al. [24] reported adhesion and diffusion wear as the predominant wear mechanisms sustained by CBN tools when turning Inconel 718. The authors evaluated speeds of 250 m/min, 350 m/min, and 450 m/min. The workpiece was subjected to high temperatures and stresses, suffering superficial plasticization. As such, the alloy spread over the contact area between the insert and the workpiece. Regarding diffusion wear mechanisms, Bushlya et al. [29] also reported that, under both high pressure and temperature, boron and nitrogen diffuse from the CBN into the Inconel 718 while forming solid solutions. A chemical reaction triggers the formation of Ti and Nb nitrides and Cr, Mo, and Nb borides. The authors also found that the presence of TiC binder in PCBN is an obstacle to further diffusional loss of the CBN phase. Despite the diffusional loss of carbon, TiC remains more stable than CBN and acts as an inert obstacle. These results made it possible to explain the significantly lower wear rate of PCBN tools with low CBN content and ceramic binder compared to the high CBN content grades.

In the present study, instrumented turning experiments were devised to evaluate the machinability of Inconel 718 alloy using PCBN tools. Two PCBN tool types were used that had distinct binder phases: TiN and TiC. The effect of the binder on the generated cutting loads and the sustained tool wear is presented and discussed. Although the use of PCBN tools for machining Inconel alloys has been researched to some extent, the influence of the binder phases could use additional exploration, as this may bring some advantages in the use of these tools, especially when aiming to mitigate common problems associated with the machining of Inconel 718.

2. Materials and Methods

Longitudinal cylindrical turning tests were performed using a Mazak Integrex i-200ST multitasking CNC machine instrumented with a load cell (Kistler 9129A piezoelectric dynamometer) coupled to a multichannel charge amplifier (Kistler 5070A) and data acquisition system (Kistler 5697A). In addition to the acquisition of the cutting forces, tool flank wear measurements and image collection of the rake and flank face were conducted using a DinoLite digital microscope. SEM images were taken, and a spectroscopy analysis was also performed. The SEM/EDS analysis was conducted using a high-resolution (Schottky) environmental scanning electron microscope with X-ray microanalysis and electron backscattered diffraction analysis (FEI Quanta 400 FEG ESEM/EDAX Genesis X4M). To avoid contaminants, all samples were submitted to an ultrasonic cleaning bath prior to the SEM analysis. The samples were immersed in ethanol and subjected to ultrasonic waves for 2 min to remove any debris or unwanted particles that may have accumulated on the surface of the samples. Table 1 displays the mechanical properties at both room temperature

(RT) and 649 °C, as specified by the alloy manufacturer and determined through tensile testing according to ASTM E8/E8M-16a and ASTM E21.

Table 1. Mechanical properties of the tested IN718 alloy as a function of temperature.

Temp.	Yield S. (MPa)	Tensile S. (Mpa)	Elongation (%)	Area Reduction (%)
RT	52.70	19.06	18.43	4.73
649 °C	50.00	rem	17.00	4.75

A schematic representation of the described experimental setup is shown in Figure 1. A tool holder (ISO DCLNL 2525M 12) was clamped to the dynamometer, resulting in an insert (ISO CNGA 120408) setting angle of 95°, a rake angle of −6.5, and a clearance angle of 6.5°. A sampling rate of 1000 Hz was defined for the three components, F_x , F_y , and F_z , which corresponded to the passive, cutting, and feed forces, respectively. Concerning the lubrication conditions, a soluble oil emulsion was used with a pressure of 3.7 bar pointed towards the cutting edge. The tested levels of each cutting parameter are presented in Table 2. The full combination of the presented parameters was used for the two different cutting inserts (with different binder phases). Experimental tests usually vary the cutting speed (v_c) from 150 to 400 m/s, so five cutting speed levels within this range were selected. A feed (f) of 0.1 and 0.2 mm/rev and a depth of cut (a_p) of 0.15 mm were selected for the experimental runs. This combination of cutting conditions resulted in a matrix of 10 tests for each tool grade, adding up to 20 different experimental runs.

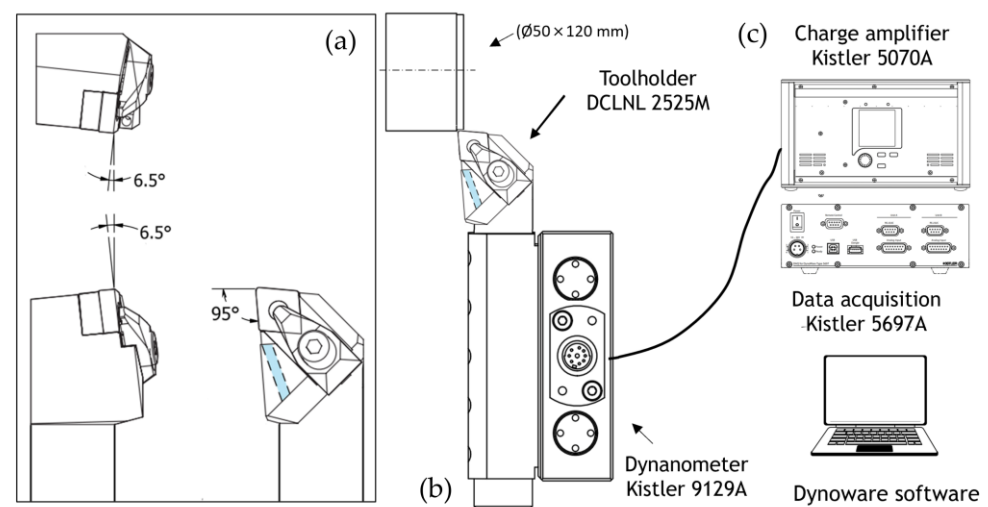


Figure 1. Instrumented setup of the longitudinal, cylindrical turning machining operations: (a) tool holder and effective rake, clearance, and cutting-edge angles; (b) cutting tool and tool holder relative to the position of the workpiece and load cell mount; (c) charge amplifier and data acquisition system.

Table 2. Tested levels for each cutting parameter.

Cutting Parameter	Levels				
Depth of cut, a_p (mm)	0.15				
Feed, f (mm)	0.1				
Cutting speed, v_c (m/min)	150	200	250	300	350

Two identical cutting inserts were selected that varied the ceramic binder: (i) titanium carbide (TiC) for the PBY603 grade and (ii) titanium nitride (TiN) for the PBY602 grade. These 50% CBN content grades are suitable for the continuous and lightly interrupted cutting of hardened steel and the finishing of abrasive high-strength cast irons, and they can also be used to machine heat-resistant superalloys. It is worth noting that the inserts were

composed of a PCBN tip brazed on a cemented carbide substrate, as shown in Figure 2. The inserts had an AlTiN/TiSiAlN double-compound coating (1.5 μm thickness) applied using the physical vapor deposition (PVD) process. Both inserts had the same negative 80° rhombic-shaped cutting insert and a honed-edge preparation with a 0.020 mm radius, which was measured (for thorough control of the cutting conditions) using the Brucker Alicona apparatus based on 3D optical measurement technology (at Palbit S.A.), as shown in Figure 2.

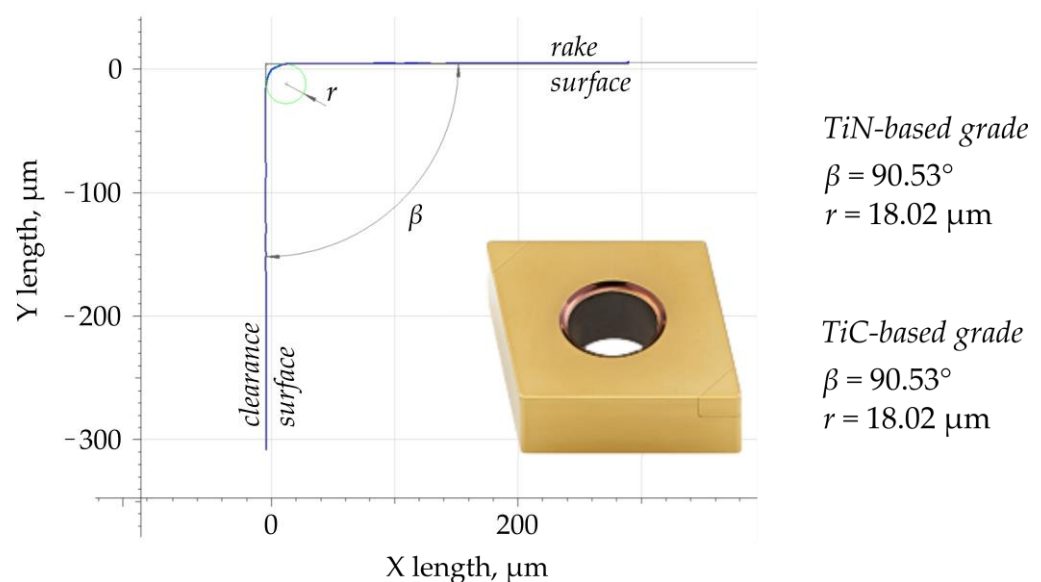


Figure 2. Overall geometry of the cutting insert (brazed tip construction) and edge radius measurement (at <0.05 mm from tool tip) of TiN-based and TiC-based PCBN inserts.

The Inconel 718 samples were equally pre-machined (facing and turning) into cylindrical shapes (50 mm in diameter), and a free length of 55 mm was defined for each longitudinal turning pass, ensuring the repeatability of the process. Prior to the machining operations, hardness tests were conducted (using an Emco M4U-075 hardness testing machine, according to ISO 6508) on the cylindrical rods. The following steps were successively repeated for each condition of the turning experiment: (i) placing a virgin (i.e., new), turning the insert on the tool holder; (ii) starting the data acquisition system without the lathe rotation; (iii) starting the turning test while acquiring data; (iv) stopping the test after a determined number of passes; (v) inspecting the tool and measuring the flank wear with a digital microscope; (vi) collecting the chip; (vii) repeating steps (i) to (iv) until a flank wear (VB_{max}) of 0.2 mm is achieved or 5 min of cutting time have been completed.

An example of the as-recorded cutting force data is shown in Figure 3. Distinct stages can be noticed. During the first stage (I), the force noise came from the lathe since the spindle was already rotating, but the cutting tool was motionless, whereas during the second stage (II) the cutting tool started its movement, entering the workpiece and beginning to cut. This second stage was characterized by a sudden increase in the forces, which stabilized less than half a second later into the (III) cutting stage itself. This third stage corresponded to the steady-state cutting conditions that were considered for this analysis. The last stage (IV) was characterized by a peak in the forces, possibly due to the fact of inertial effects and occasional chip tangling and winding around the workpiece.

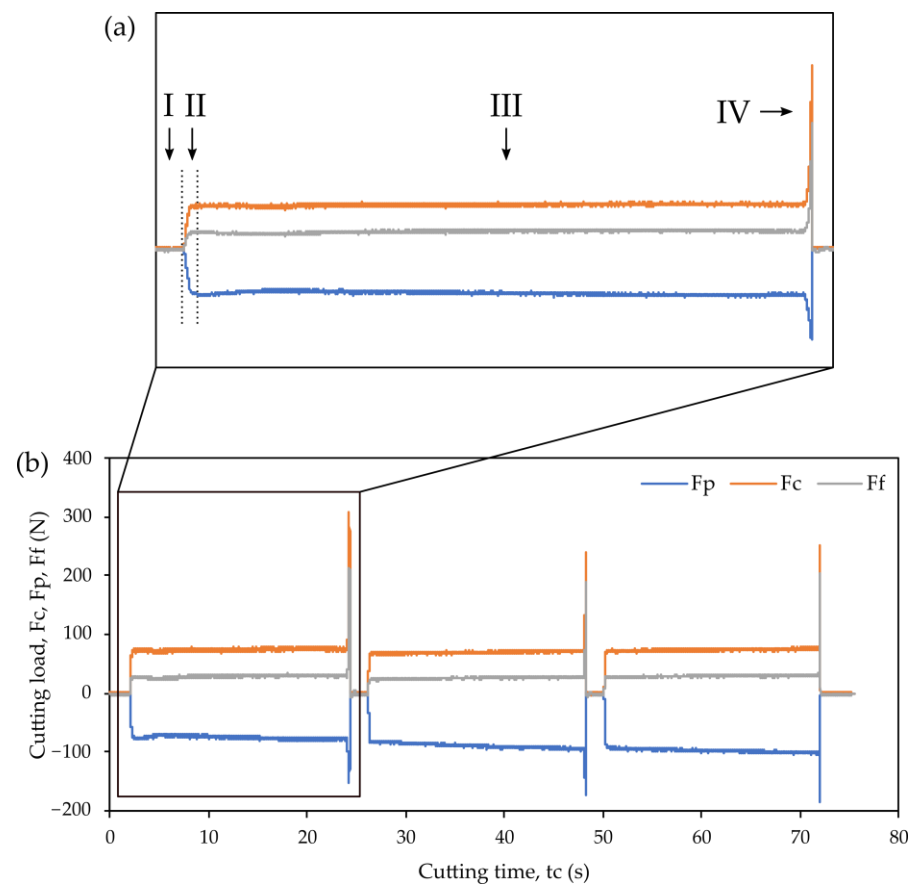


Figure 3. Load evolution of the Inconel 718 turning operation using the TiC binder cutting tool ($v_c = 200$ m/min, $f = 0.10$ mm/rev, and $a_p = 0.15$ mm) while recording the cutting force signals: continuous cutting of (a) multiple (3) longitudinal turning passages; (b) distinct stages in each passage.

3. Results and Discussion

3.1. Workpiece Material Inspection Analysis

A chemical composition analysis enabled a comparison with material standards, confirming its compliance, as depicted in Table 3. Moreover, small samples of Inconel 718 were prepared for microstructural observation. After polishing (as seen in Figure 4a), these samples were chemically etched with oxalic acid, enabling different phases and grain structures, as shown in Figure 4b. Large carbide particles (1 to 7 μm) can be seen in the unetched sample, which are responsible for the hardened condition along with the very fine precipitates [32] dispersed along the matrix. The microstructure shows equiaxed grains and annealing twins, suggesting a recrystallized structure [33,34]. In terms of the hardness, different measurements were performed for different radial distances to the center of the cylindrical samples. No significant changes in hardness were noticed along the diameter of the samples (44.1 ± 0.1 HRC).

Table 3. Chemical composition (wt.%) of the Inconel 718 alloy processed in the current study.

Element	Ni	Fe	Cr	Nb	Mo	Ti	Al	W	Si	Co
Measured	52.70	19.06	18.43	4.73	3.00	1.02	0.541	0.114	0.114	0.109
Standard min.	50.00	rem	17.00	4.75	2.80	0.65	0.20	-	-	-
Standard max.	55.00	-	21.00	5.50	3.30	1.15	0.80	0.35	0.35	1.00

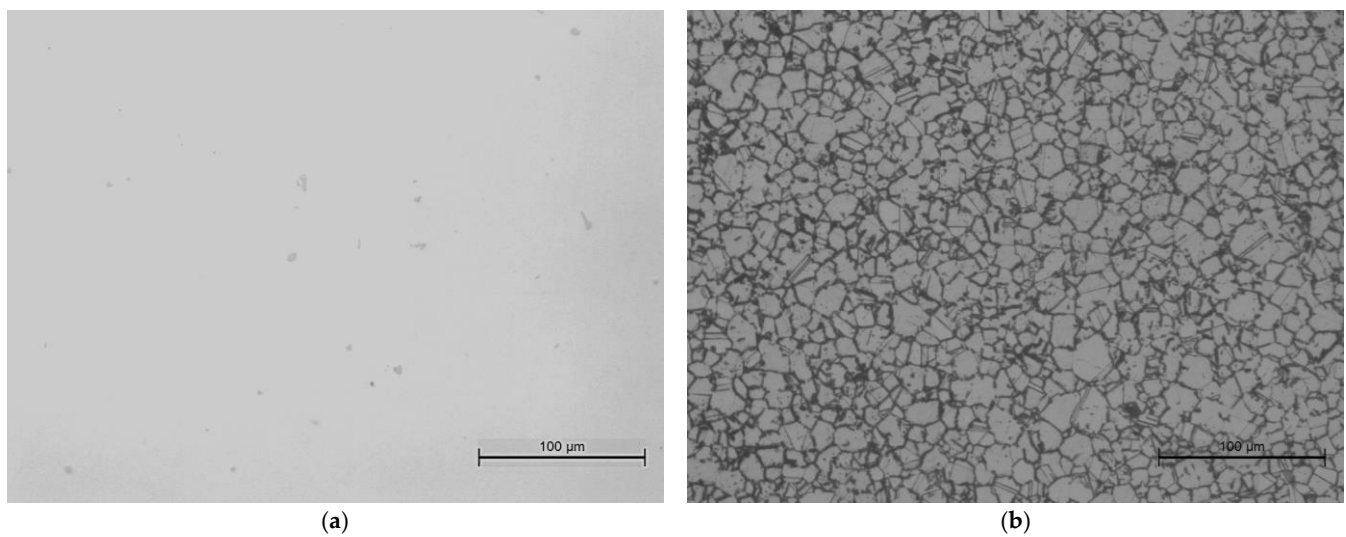


Figure 4. Optical microscopic images of Inconel 718: (a) polished condition evidencing the occurrence of large precipitates; (b) chemically etched (oxalic acid) condition, evidencing the microstructure.

3.2. Cutting Load

Figure 5 allows for the observation of the cutting loads according to each selected operational condition. The significant evolution of these loads can be noticed for each selection of cutting parameters due to the considerable wear rates promoted by the low machinability of the alloy. The initial force values, which were minimum due to the fact of insignificant tool wear, are represented by “min.”, whereas “max.” illustrates the last passage load values, which were maximum due to the fact of tool degradation. The average force values over the entire test are represented by “avg.”. Overall, the highest values were achieved by the passive force component (F_p) followed by the cutting force (F_c) and feed force (F_f), in descending order, given that when the depth of cut is smaller than the nose radius of the tool, the passive or radial component of the tool forces is found to be most dominant [24,25,29,35,36]. Moreover, passive force had a large evolution over time, often amounting to triple and even quadruple the initial (i.e., virgin tool) value, when reaching the end of the tool’s life. Monitoring the evolution of this force can provide relevant information on the tool wear evolution. The force appears to be highly sensitive to the evolution of the tool wear and degradation of the tool edge surface, which is a tendency also observed by other researchers [24,35,37]. In addition, the passive force seems to be associated to the ploughing force, which is caused by the flow of material ploughed by the clearance face of the tool due to the elastic deformation of the workpiece material under the clearance surface [35].

The first pass cutting forces for each tool, cutting speed, and feed are shown in Figure 6 for each distinct cutting tool. This first pass values are important, since at this point the cutting tools have the most similar wear conditions, enabling a more suitable comparison of the cutting forces. As expected, higher cutting forces were achieved when machining with higher feeds for both tools, given that maintaining the depth of cut and increasing the feed results in a higher chip cross-sectional area along with higher cutting forces. It is important to note the high stability of the cutting forces in the steady-state regime (standard deviation < 5 N). When varying the feed from 0.1 mm/rev to 0.2 mm/rev and cutting with the TiC binder inserts, this resulted in an average increase of 52.1% in the cutting forces, while under the same conditions, an increase of 55.5% was observed when machining with the TiN binder inserts. The cutting forces proved to have a slightly decreasing tendency when increasing the cutting speed. As the cutting speed increased, there was a larger energy input in the machining process, which combined with the lower heat diffusion (near-adiabatic process), promoted a temperature increase that resulted in thermal softening of the workpiece material. For the tests, it was not possible to perceive a

significant difference in the cutting forces among the distinct CBN binders. Regardless of the employed cutting insert, the measured load values oscillated at approximately 120 N when machining with a feed of 0.2 mm/rev and 80 N with a feed of 0.1 mm/rev.

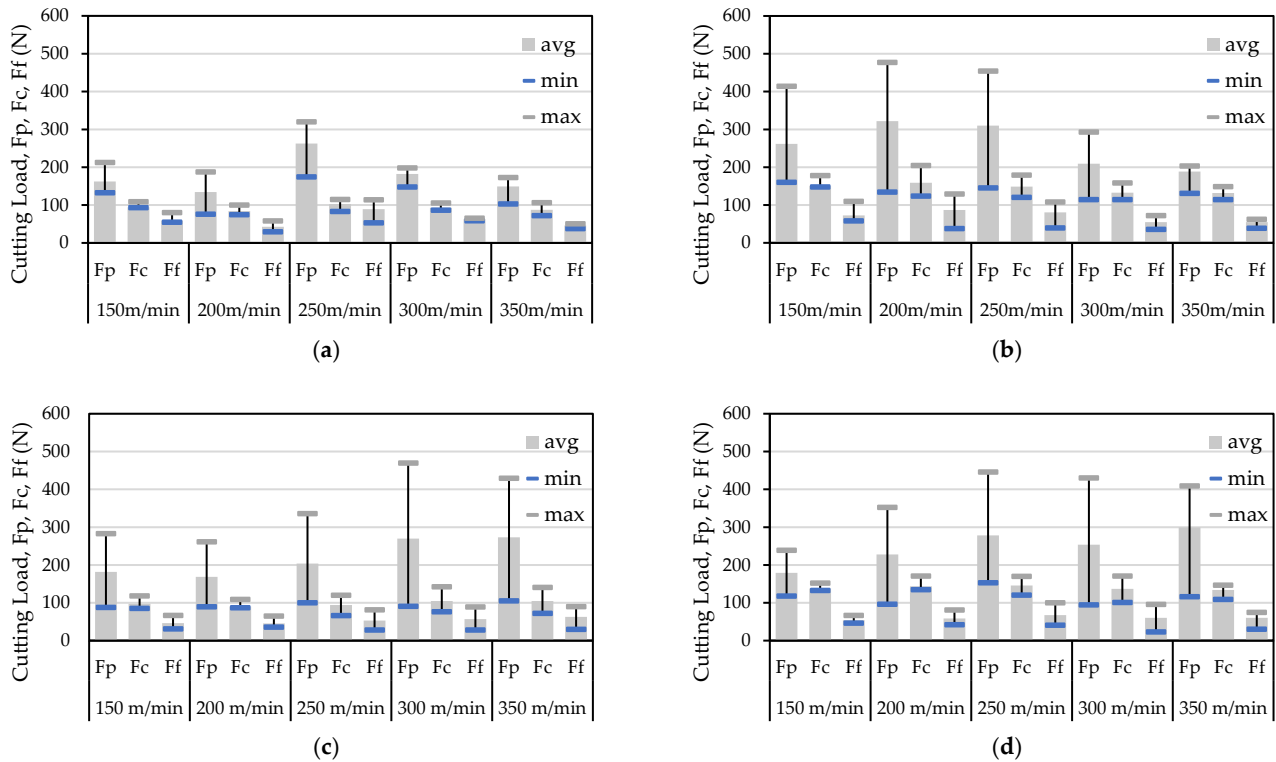


Figure 5. Cutting load evolution according to the selected cutting parameters and depending on the first (min.) and last (max.) cutting tool passages: (a) TiC binder cutting tool and $f = 0.1$ mm/rev; (b) TiC binder cutting tool and $f = 0.2$ mm/rev; (c) TiN binder cutting tool and $f = 0.1$ mm/rev; (d) TiN binder cutting tool and $f = 0.1$ mm/rev.

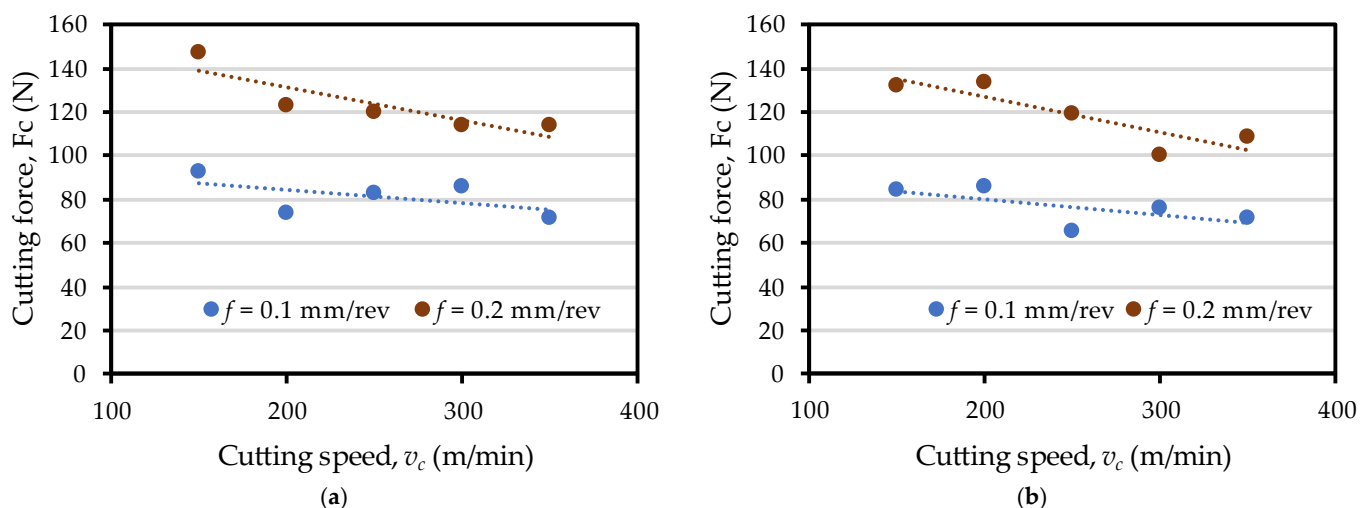


Figure 6. Measured cutting forces on the initial passage of each tool for each tested configuration of cutting parameters: (a) TiC binder cutting tool; (b) TiN binder cutting tool.

The measurement of the first pass cutting forces enabled the calculation of the specific cutting pressure, K_c , which is a highly relevant parameter used for the evaluation of a material's machinability and enables an estimate of the cutting force for scenarios with

distinct operational conditions. The specific cutting pressure can be defined as the ratio between the main cutting force and cross-sectional area of an undeformed chip, A_0 . The cross-sectional area of the undeformed chip can be calculated using Equation (1), and the specific cutting pressure, K_c , can be calculated using Equation (2).

$$A = a_p \cdot f \quad (1)$$

$$K_c = \frac{F_C}{A} \quad (2)$$

Figure 7 exhibits the evolution of the specific cutting pressure according to the feed conditions. Typically, K_c exponentially increases for a smaller chip section while stabilizing when increasing the chip section, which is a phenomenon associated with size effects in metal cutting, as widely observed by researchers [35,38,39]. The occurrence of defects in metals, such as grain boundaries or missing atoms, is generally acknowledged, and the chance of encountering such stress-reducing defects increases for larger sizes of removed material [39]. In addition, the occurrence of ploughing for increasingly smaller feed rates explains the size effect. When the uncut chip thickness becomes smaller or similar to the tool edge radius, the cutting loads did not decrease proportionally due to the considerable relative contribution of workpiece deformation (compression), leading to higher K_c values.

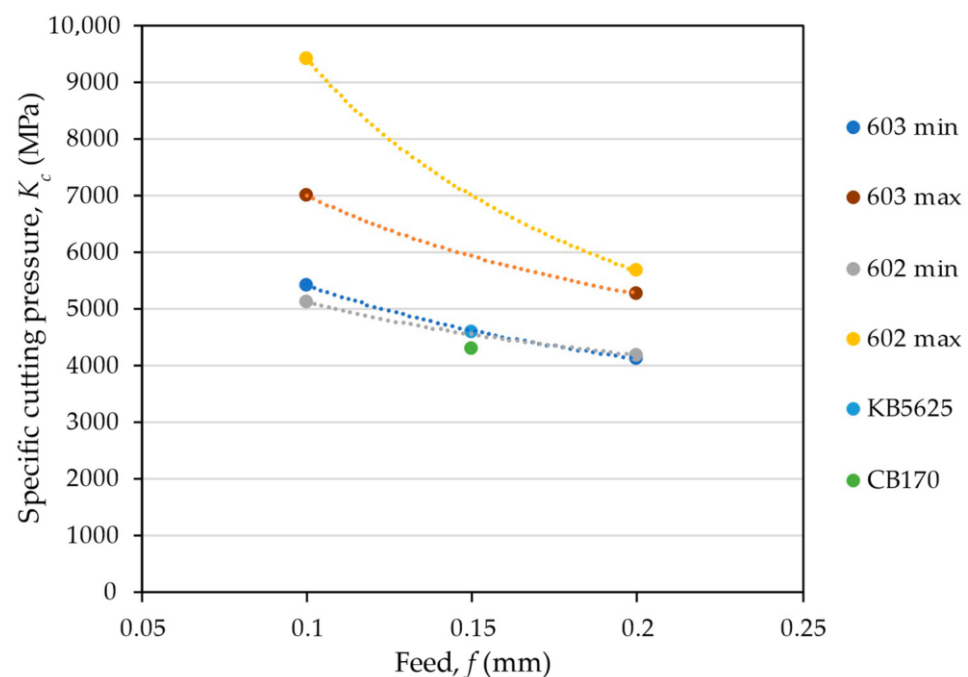


Figure 7. Specific cutting pressure values considering new and used tools and their comparison with values in the literature for similar cutting insert geometries.

The turning tests comprised two different chip cross-sectional areas, with the highest values of cutting pressure being achieved for the lowest feed, which corresponded to the smaller chip section, as explained by the size effect in the metal cutting. Values between 4000 and 5500 N/mm² were obtained for a feed of 0.2 and 0.1 mm/rev, respectively, at a cutting speed of 300 m/min and depth of cut of 0.15 mm. These are typical values for Inconel 718 turning processes with negative rake angles (commonly used for Ni-based alloys), hence, inducing high values of specific cutting forces. Furthermore, Cantero et al. [35] obtained similar K_c values when turning Inconel 718 (45 HRC) with commercially available KB5625 and CBN170 PCBN inserts. These inserts have a medium CBN content and ceramic binder, with a honed edge preparation (25 μ m) similar to the tested tools in this work. Whereas in Figure 7 the specific cutting pressure labeled with “min.” corresponds to the

first passage of the longitudinal turning (i.e., virgin cutting insert), “max.” corresponds to the last passage of that insert. Significantly higher specific cutting pressures (>30%) occur when reaching the tool’s end of life, proving that the wear affects the cutting power, leading to a less efficient machining along with a higher surface roughness of the part, thus affecting the process sustainability and overall quality of the generated surface.

3.3. Tool Wear

The adopted experimental procedure made possible the tracking of the evolution of the tool wear. It is an inevitable, gradual, and complex phenomenon affecting workpiece surface accuracy and integrity and contributing to the cost of the machining process. It occurs due to the fact of geometrical damage, frictional force, and temperature increases at the tool–workpiece interface region. Studying the influence of the cutting parameters and their effect on tool wear allows to optimize the process, achieving both better results on the final product and on the economical side of the operation.

To establish the tool flank wear progression depending on the machining time, wear data were acquired approximately every 30 to 60 s of the machining time. To do so, the test was stopped and the flank wears (VB_{max} and VB_{notch}) were measured according to ISO 3685. Herein, flank wear refers to VB for simplicity. Figure 8 shows the monotonic linear wear increase for the CBN cutting tool according to the cutting time (t_c). These data were then computed into a graph, where the ratio of VB and cutting time represents the tool flank wear rate (TW_f) in mm/s, as presented in Figure 8.

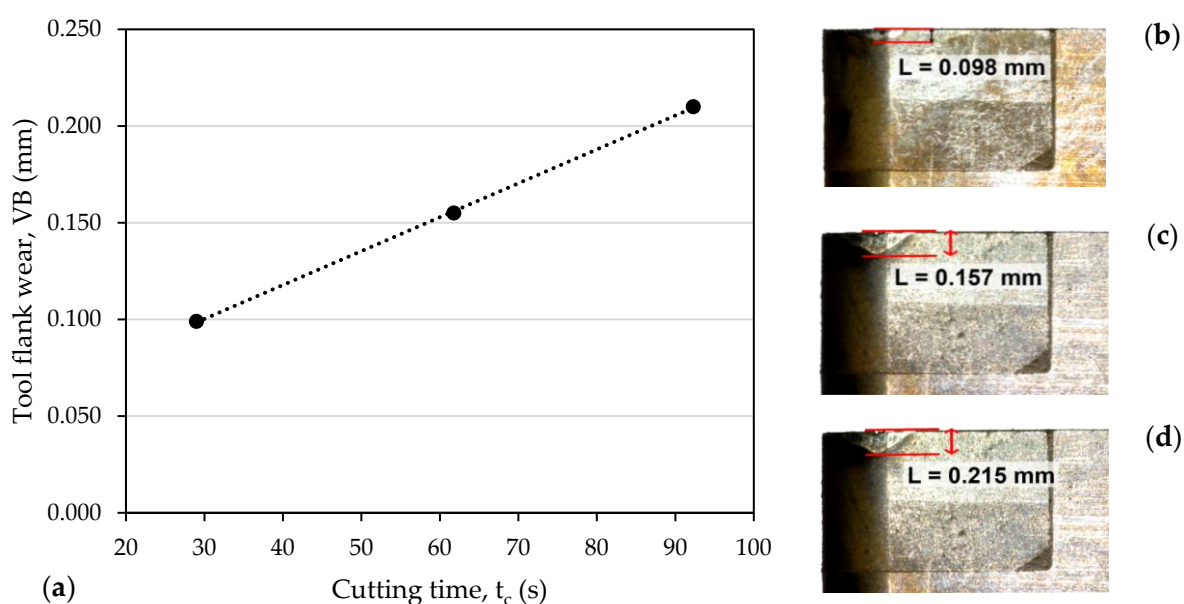


Figure 8. Tool flank wear evolution (a) as a function of the cutting time for a cutting speed (v_c) of 300 m/min and feed (f) of 0.2 mm using a TiC binder insert: (b) flank face for a cutting time of 30 s; (c) flank face for a cutting time of 62 s; (d) flank face for a cutting time of 92 s.

As the cutting speed increased, the tool wear rate tended to increase as well, which may be explained by the increase in the cutting temperature at the cutting edge for increasing cutting speeds. Those high-speed (and, thus, high-temperature) conditions may lead to softening of the tool material which, in turn, may result in an accelerated tool wear rate (monotonic trend of the curves shown in Figure 9). Still, there seems to be a tendency towards the stabilization of the wear rates for longer cutting speeds. This might be associated with the obtained cutting loads that were more stable for faster cutting speeds (refer to Figure 5), especially for TiC binders. Thus, it is noticeable that within cutting speeds between 250 m/min and 350 m/min, the wear rate tended to a steadier rate when machining with TiC binder inserts. However, when machining the same alloy with the

CBN tool with TiN binder, this effect was less evident, since the tool flank wear rate kept increasing with an increasing cutting speed, while the cutting loads also showed lower stability ($F_p \gg F_c, F_f$), as illustrated in Figure 5.

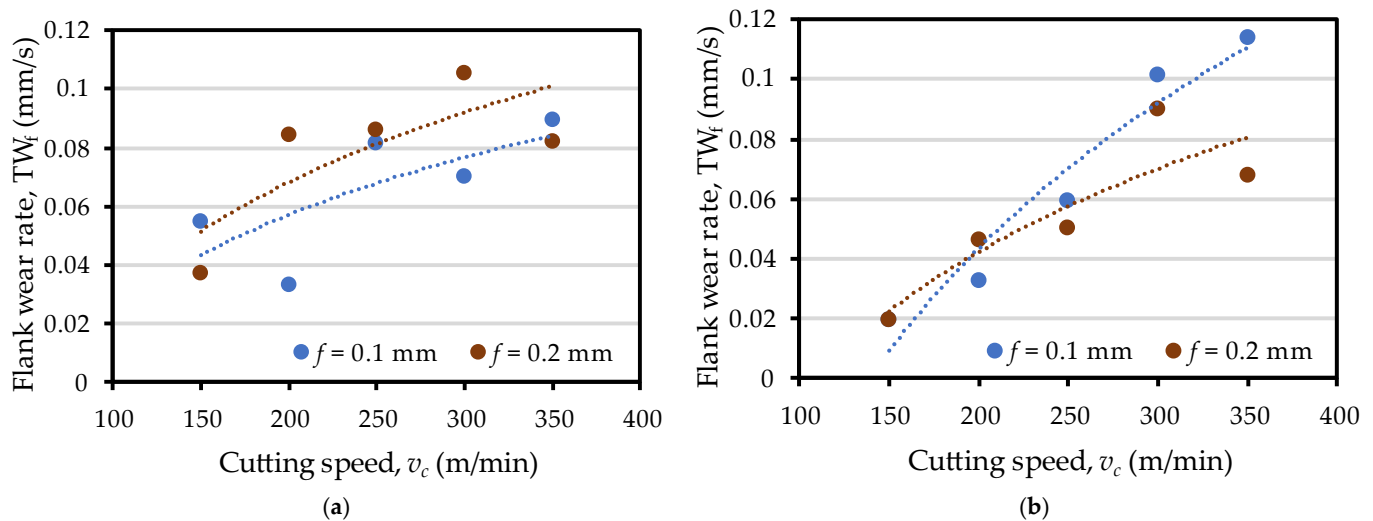


Figure 9. Influence of the cutting speed (v_c) on the tool flank wear rate for each distinct tested insert: (a) TiC binder; (b) TiN binder.

Throughout the tests, all inserts experienced noticeable crater wear on the rake face and flank wear due to the fact of abrasion on the flank face. In most of the experimental runs, an increased cutting speed improved the stability of the cut. In Figure 10, two distinguishable wear patterns that were often found in the current experiment are shown. At lower cutting speeds (i.e., between 150 and 200 m/min), the flank wear was extremely irregular with the length variations of the flank itself in addition to the formation of build-up edge and notching. At higher cutting speeds, despite the rapid wear of the tool, this phenomenon was less discernible. Regarding the influence of the feed on flank wear, the results do not show a noticeable influence for the different levels of tested feeds (0.1 and 0.2 mm/rev), which is supported by Cantero et al. [35], who found similar results when machining 45 HRC Inconel 718.

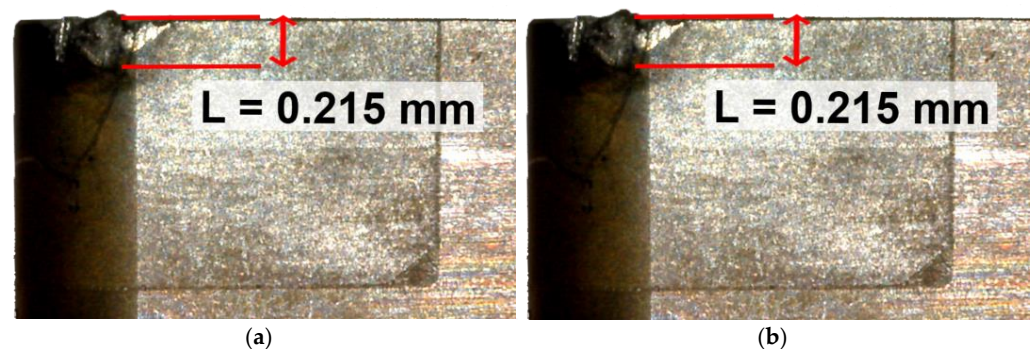


Figure 10. Example of cutting inserts (TiC binder) with exceeded flank wear ($V_B > 0.2$ mm) for different operational cutting conditions: (a) cutting speed (v_c) of 200 m/min and feed (f) of 0.2 mm; (b) cutting speed (v_c) of 350 m/min and feed (f) of 0.2 mm.

Knowing the speed at which each tool flank degrades, the flank wear rate, as shown in Figure 9, enables the calculation of the expected tool life, as presented in Figure 11, using a flank wear of 0.2 mm as the wear criterion. It was chosen to display the average tool life of each tool for both feeds, as no minor differences were found for the flank wear with the two tested feeds (0.1 and 0.2 mm/rev). It is also important to note that the tool life at a cutting

speed of 150 m/min was extrapolated and could hardly be achieved due to the chipping and notching phenomena, which is further addressed. Moreover, it is important to remark that even though the cutting speed greatly affects the tool life (which shows considerable differences regarding the CBN binder at low cutting speed), it plateaus at 300 m/min. This could be explained by a change in the phenomena, leading the wear to change from a tribological type (i.e., abrasion and adhesion) to a chemical (i.e., diffusion and oxidation). Within the selected range of the tested parameters, the cutting speeds between 250 and 350 m/min resulted in smaller notching, better cutting stability, and chip control despite a short tool life.

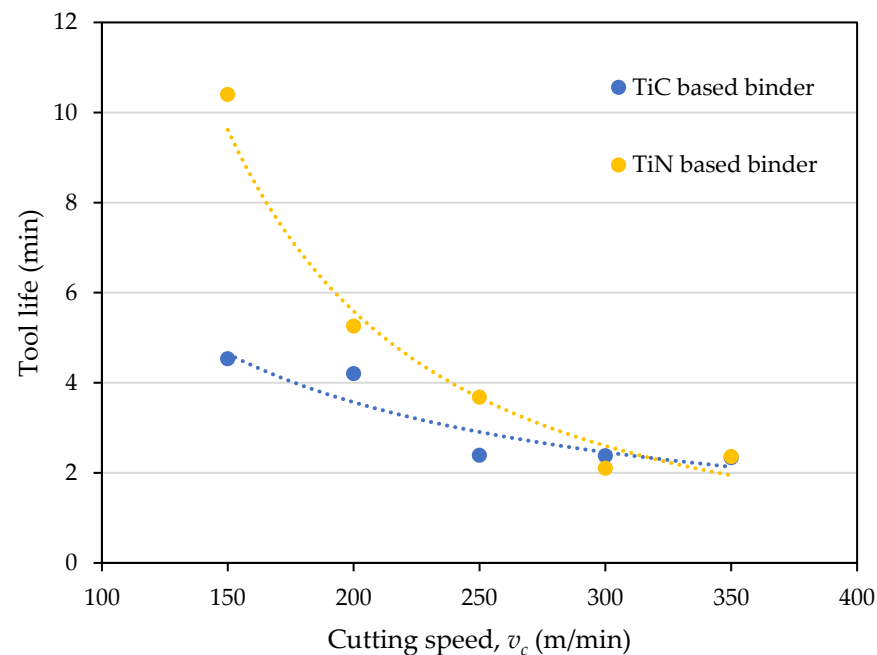


Figure 11. Influence of cutting speed on tool life prediction based on a maximum flank wear of 0.2 mm for TiC and TiN based binders.

Productivity should not only be assessed by the geometric parameters of the operation (which allow to calculate the MRR) but also in terms of the tool's life, particularly at an industrial level where tool replacement and set-up times are detrimental. Figure 12 exhibits the removed material volume as a function of the feed and cutting speed for the maximum tool life ($VB > 0.2$ mm), enabling an assessment of the tool's performance.

Figure 12 allows for the observation of two distinct conclusions: (i) the highest machined volume was achieved with a feed of 0.2 mm and (ii) the high material removal rates did not necessarily correspond to a lower machined volume (due to the shorter life), constituting improved productivity scenarios.

Notch wear induced by chipping, contrary to flank wear, decreased with an increase in the cutting speed and became indistinguishable from flank wear at $v_c = 250$ m/min, which was also reported by several other authors, for the same tool–workpiece material pairs [35,40]. The notching and built-up edge were particularly intense at lower cutting speeds for both tested feeds with the TiC binder insert, as seen in Figure 13, whereas with the TiN binder inserts under the same cutting conditions, less notching occurred. This excessive notch wear at lower cutting speeds led to an accelerated deterioration of the cutting edge and its ability to maintain strength properties, culminating in either (i) premature failure of the tool or (ii) flank wear homogenization covering the initial notching. The second occurrence is a more convenient scenario, resulting in a more gradual tool wear and, thus, the higher stability of the cutting operation. This is consistent with the fact that the tool flank wear pattern is more homogenous at higher cutting speeds, becoming the failure mode for most tools at speeds above 200 m/min. Unexpected tool failure in addition to

an increasing frequency of tool change may also destroy the previously machined surface, causing an inherent impact on the economical side of the process.

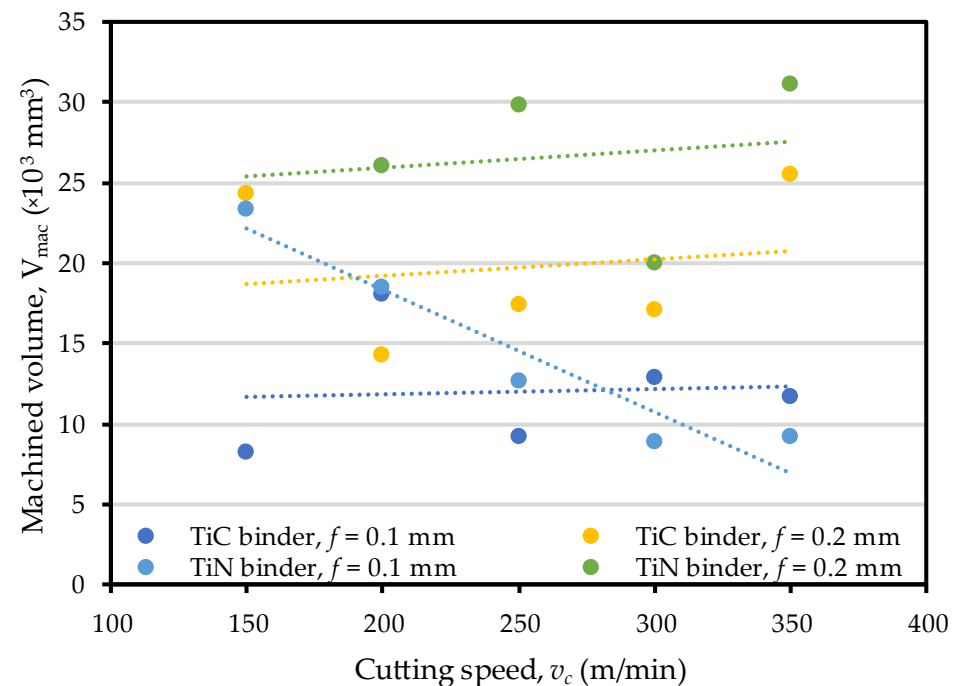


Figure 12. Influence of the cutting speed, feed, and PCBN binder on the machined volume.

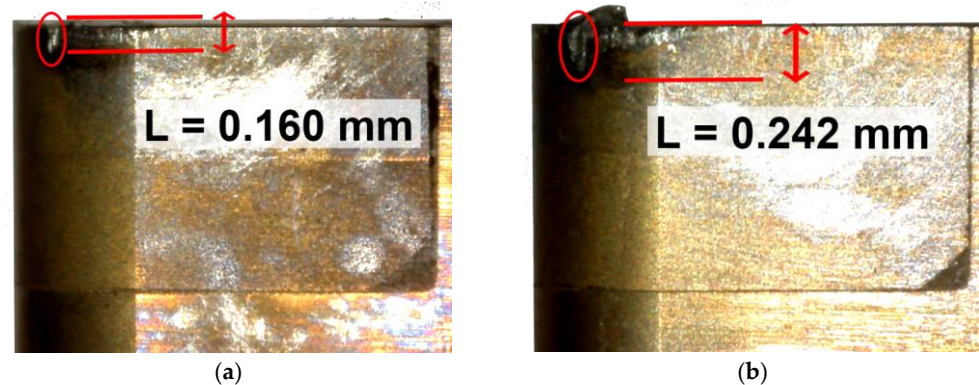


Figure 13. Flank surface of the TiC binder insert exhibiting notching under a cutting speed (v_c) of 150 m/min and (a) feed (f) of 0.1 mm after 105 s of cutting; (b) feed (f) of 0.2 mm after 65 s of cutting time.

Tool failure due to the fact of notching located at the depth of cut (see Figure 14c) at cutting speeds within the range of 150–200 m/min and a reduction of notching as the cutting speed increases has also been reported by various authors [26,41]. This tool nose notching at the depth of cut is located at the intersection between the cutting edge and the machined surface, which is a common failure mode when machining nickel-based alloys. Notch formation results from a combination of aggressive cutting conditions involved during the machining process of Ni-based alloys: high temperature, elevated strength, and strain hardening of the workpiece maintained at high temperature and the abrasive chips [42].

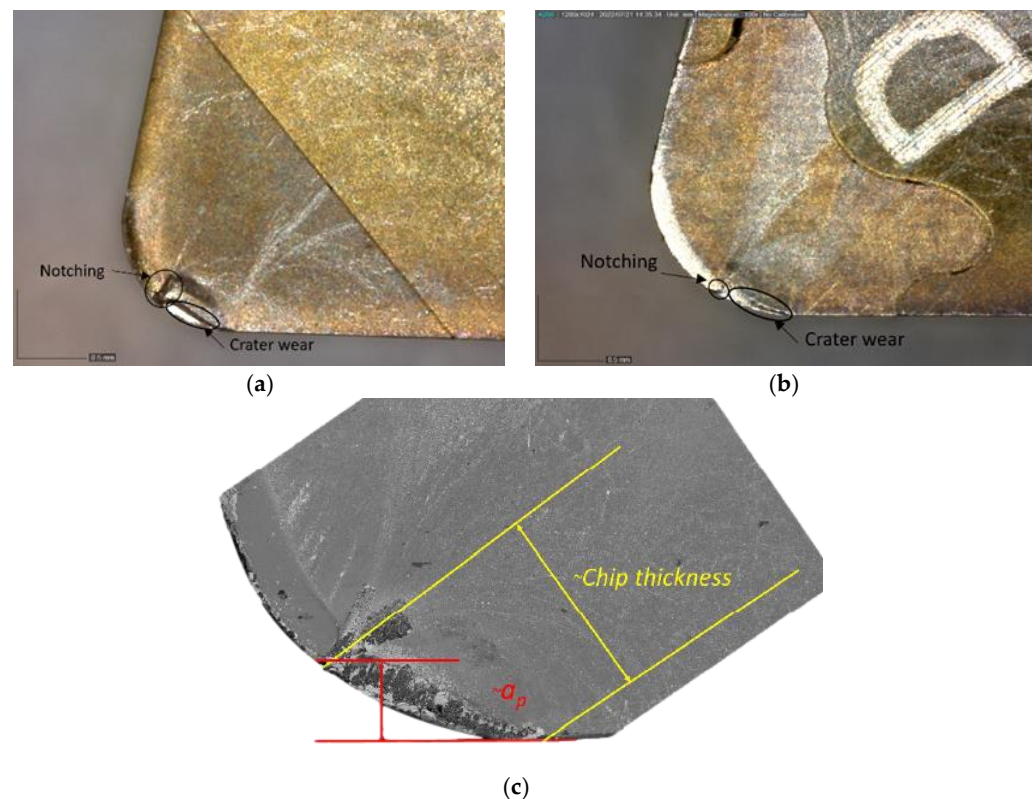


Figure 14. Rake face after 1.5 min of machining time: (a) insert 603; (b) insert 602; (c) notching occurrence located at depth of cut dimension.

Comparing the tool wear with the TiN binder insert and the TiC binder insert, during the previous turning experiments, it seemed that the first one appeared to have a more homogenous and predictable flank wear. The flank wear rate (TWf) of insert 602 showed less variation than insert 603 for the two tested feeds, except at a cutting speed of 350 m/min, so a further investigation and comparison of these two inserts was performed.

Table 4 shows the measured flank wear (VB) for cutting speeds of 250 m/min and feed of 0.1 mm, confirming that TiN binder inserts outperform TiC binder inserts, achieving less flank wear. The rake face images shown in Figure 14 also support the initial premise that the TiC binder insert has a tendency to notch at the depth-of-cut line. The TiN binder inserts outperformed TiC by almost 30%, a value that is in line with the 20% difference reported in the studies by Bushlya et al. [40] when machining Inconel 718 under flood coolant lubrication cutting conditions at a cutting speed of 300 m/min, feed of 0.1 mm/rev, and depth of cut of 0.3 mm. Curiously, it was reported that the oxidation of TiN and TiC start at 700 °C and 800 °C, respectively, forming TiO₂ [43].

Table 4. Flank wear after machining for 1.5 min for v_c of 250 m/min and f of 0.1 mm.

Insert	VB			Average
	#1	#2	#3	
TiC	0.099	0.082	0.085	0.089
TiN	0.089	0.061	0.058	0.069

Electron backscatter diffraction (EBSD) imaging was used to further investigate and distinguish compositional changes in the tools tested. Different zones usually have different light intensities that correspond to distinct chemical compositions. EDS analyses and SEM images allowed to identify compositional changes on the tool's surface, such as the build-up edge, and to recognize that, as consequence of the abrasion at the tool–workpiece interface,

small portions of the workpiece tended to become attached to the tool while the coating was removed.

Figures 15 and 16 exhibit SEM images of the three TiC and TiN binder inserts used to machine alloy 718. All tested inserts exhibited a curvilinear, elongated branded zone where the chip primarily exited at the rake face, resulting in both a loss of the tool coating due to the tool–chip interaction, diffusion, and adhesion of workpiece elements. Regarding the TiC and TiN inserts, there was a noticeable difference among them, which is visible as prominent abrasion wear roughly in the same place on the three TiC inserts, and this is coincident with the notching present on the flank face, as seen in Figure 17. This excessive notching tendency of the TiC binder insert compared to the TiN binder insert has previously been noticed in tool wear rate analyses and further confirmed with SEM analysis.

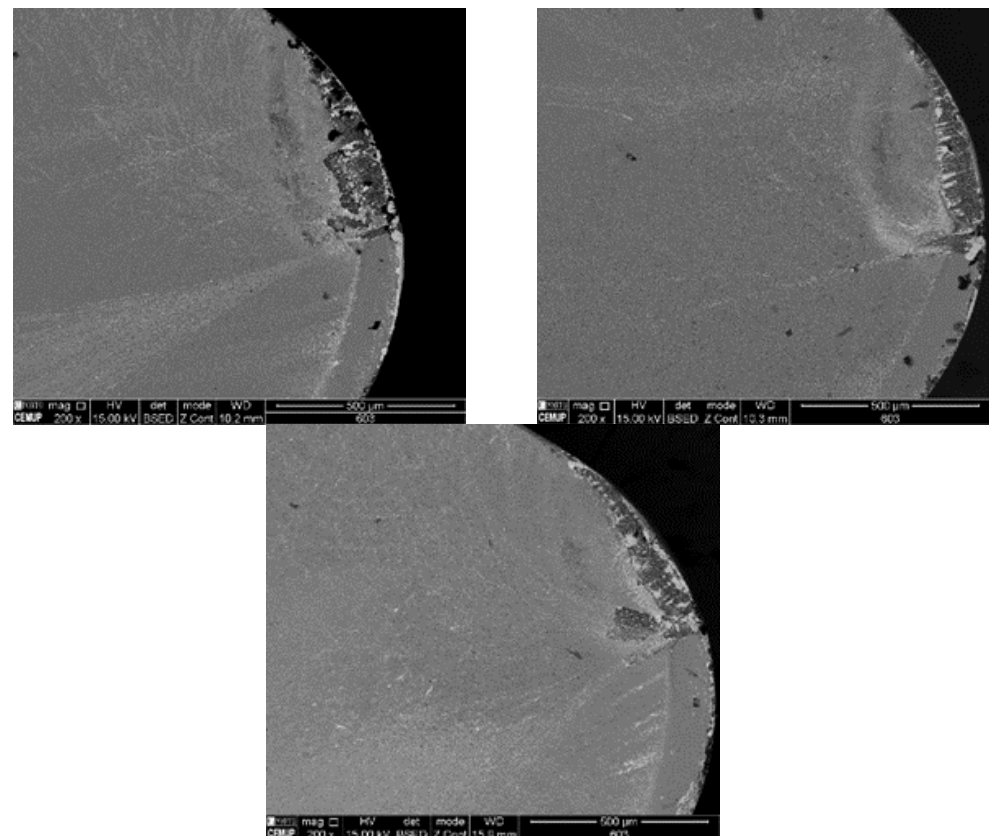


Figure 15. SEM images of the TiC binder insert rake face after 1.5 min of machining.

In addition, the flank wear on the TiN binder inserts was generally more homogeneous than for the TiC binder inserts mainly due to the absence of notching. Moreover, SEM images made it possible to understand that the cutting edge of the TiC binder inserts underwent more workpiece adhesion than the TiN binder inserts. While the workpiece material adhered to the tool, a new edge was created resulting in the loss of geometric and mechanical characteristics. This newly generated layer made the cutting edge less sharp, thus increasing the forces during the cutting, particularly the passive or radial force.

The TiN binder inserts seemed to have a geometrically consistent wear pattern on the rake face and tool, and the TiC binder insert's crater wear appeared to be darker in the images, indicating the presence of greater erosion, consequently reaching the tool's substrate. Both inserts show groove occurrence roughly at the same location, which seems to be related with the cutting depth; although for the TiC binder inserts, the cutting edge appeared to be more affected by the chipping, for the TiN binder inserts, the cutting edge seemed to better withstand its geometrical characteristics.

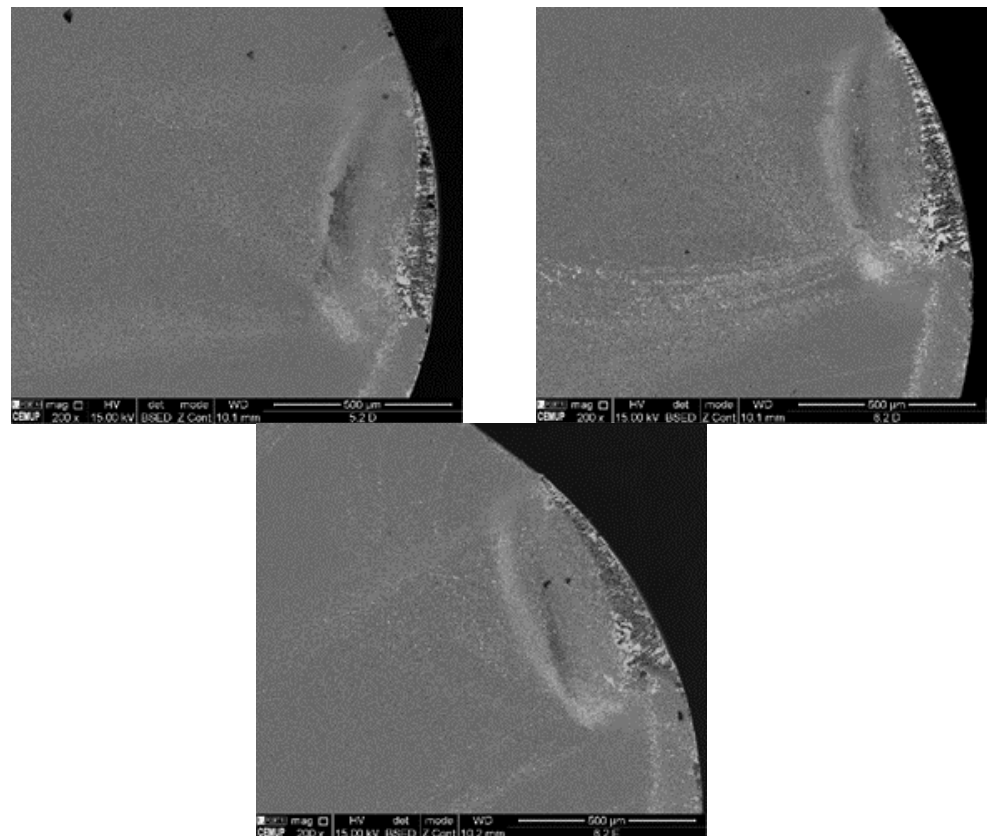


Figure 16. SEM images of the TiN binder insert rake face after 1.5 min of machining.

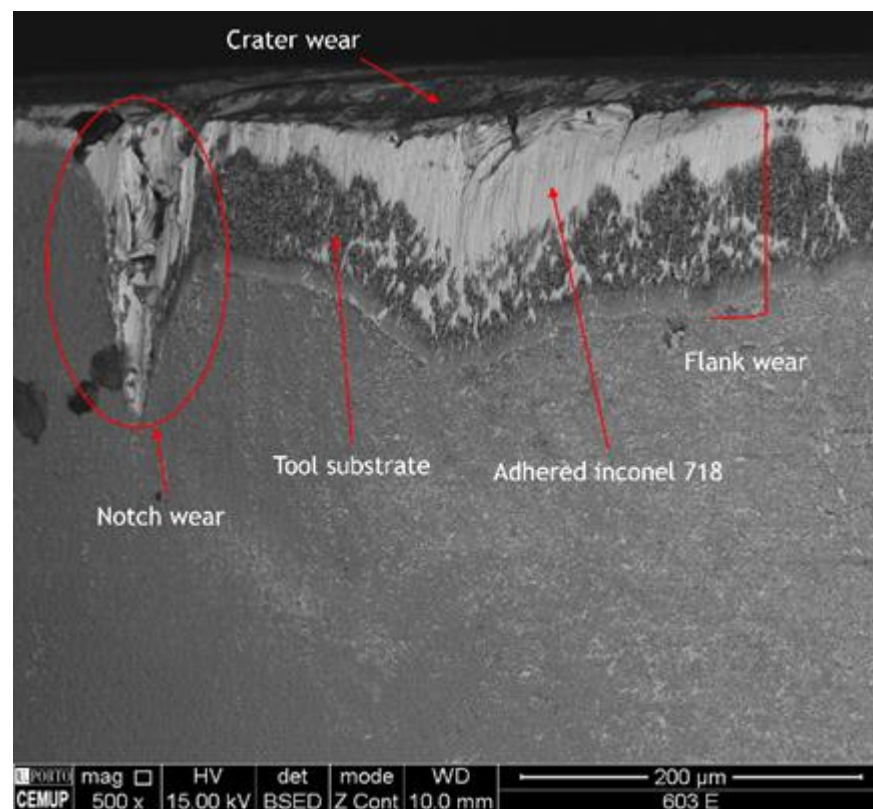


Figure 17. SEM image of a worn TiC binder insert tool flank.

4. Conclusions

In this study, instrumented turning experiments to assess the machinability of Inconel 718 alloy using PCBN cutting tools and two different binder phases, TiN and TiC, were selected. The primary cutting force displayed a consistent and gradual increase in magnitude as the depth of cut and feed rate increased, confirming the expected relationship between the machining process and operational conditions. In other words, the observed increase in the cutting force with an increasing depth of cut and feed rate was consistent with the predicted geometric relationship between these factors and the machining process. The following are the key findings:

- In terms of the cutting forces, there is a clear dependence between the obtained values and the adopted cutting parameters. The main cutting force increases for higher feed rates and decreases for higher cutting speeds;
- Increasing the cutting speed ($v_c > 300$ m/min) seems to promote a change in the dominant wear mode, from mechanical abrasion to chemical diffusion, as evidenced by the type of tool wear noticed in the cutting tools;
- Low-content PCBN tools are suitable to machine Inconel 718 at high cutting speeds ($250 < v_c < 350$ m/min) and low depth of cut (0.15 mm). At lower cutting speeds ($150 < v_c < 200$ m/min), notching and chipping are the main causes of wear, resulting in instability of the cutting operation and leading to unpredictable tool failure. At high cutting speeds, adhesion and diffusion of Inconel 718 into the tool surface deteriorate the cutting edge's geometry and toughness;
- Lower cutting speeds and the lack of chip breaker resulted in poor chip control at low cutting speeds, and there was a tendency of chips to entangle around the workpiece. Increasing the cutting speed was favorable to the appearance of the chip segmentation;
- Of all forces involved in the turning operation, passive force was the greatest, which is typical when the depth of cut is smaller than the nose radius of the tool, and showed an evolution that was close with the increase in tool wear;
- The results of the experiment indicate that a higher removal rate does not always lead to a corresponding decrease in the durability of the cutting tool, which may ultimately enable more productive cutting conditions in terms of productivity. This highlights the potential of using PCBN tools when turning Inconel 718;
- TiN binder seemed to improve the tool resistance when machining this superalloy; yet, more experiments should be conducted, particularly focusing on the evaluation of the tool's thermal evolution through combined approaches of in situ temperature measurement and numerical modeling allowing for an assessment of the wear performance and stability for different ranges of temperature (promoted by distinct operational conditions). The chemical stability of the tested tools can also be assessed under distinct lubrication conditions.

Author Contributions: Conceptualization, A.M.P.d.J. and T.E.F.S.; methodology, T.E.F.S.; software, F.M. (Francisco Matos); validation, D.F., F.M. (Francisco Marques) and A.M.P.d.J.; formal analysis, A.M.P.d.J.; investigation, F.M. (Francisco Matos); resources, D.F. and F.M. (Francisco Marques); data curation, F.M. (Francisco Matos); writing—original draft preparation, T.E.F.S., V.F.C.S. and F.M. (Francisco Matos); writing—review and editing, T.E.F.S., V.F.C.S. and F.J.G.S.; visualization, F.M. (Francisco Marques), A.M.P.d.J. and F.J.G.S.; supervision, A.M.P.d.J. and F.J.G.S. All authors have read and agreed to the published version of the manuscript.

Funding: The authors gratefully acknowledge the funding from Project Hi-rEV—Recuperação do Setor de Componentes Automóveis (C644864375-00000002), cofinanced by Plano de Recuperação e Resiliência (PRR), República Portuguesa, through NextGeneration EU.

Institutional Review Board Statement: Not applicable.

Informed Consent Statement: Not applicable.

Data Availability Statement: The data presented in this study are available on request from the corresponding author.

Conflicts of Interest: The authors declare no conflict of interest.

References

1. Mouritz, A.P. Introduction to aerospace materials. In *Introduction to Aerospace Materials*; Woodhead Publishing: Sawston, UK, 2012; pp. 1–14.
2. Choudhury, I.A.; El-Baradie, M.A. Machinability of nickel-base super alloys: A general review. *J. Mater. Process. Technol.* **1998**, *77*, 278–284. [\[CrossRef\]](#)
3. Buddaraju, K.M.; Sastry, G.R.K.; Kosaraju, S. A review on turning of Inconel alloys. *Mater. Today Proc.* **2021**, *44*, 2645–2652. [\[CrossRef\]](#)
4. Ulutan, D.; Ozel, T. Machining induced surface integrity in titanium and nickel alloys: A review. *Int. J. Mach. Tools Manuf.* **2011**, *51*, 250–280. [\[CrossRef\]](#)
5. Asala, G.; Andersson, J.; Ojo, O.A. A study of the dynamic impact behaviour of IN 718 and ATI 718Plus[®] superalloys. *Philos. Mag.* **2019**, *99*, 419–437. [\[CrossRef\]](#)
6. Shalaby, M.A.; Veldhuis, S.C. Tool wear and chip formation during dry high speed turning of direct aged Inconel 718 aerospace superalloy using different ceramic tools. *J. Eng. Tribol.* **2019**, *233*, 1127–1136. [\[CrossRef\]](#)
7. Zhou, J.; Bushlya, V.; Avdovic, P.; Ståhl, J.E. Study of surface quality in high speed turning of Inconel 718 with uncoated and coated CBN tools. *Int. J. Adv. Manuf. Technol.* **2012**, *58*, 141–151. [\[CrossRef\]](#)
8. Agmell, M.; Bushlya, V.; M'saoubi, R.; Gutnichenko, O.; Zaporozhets, O.; Laakso, S.V.; Ståhl, J.-E. Investigation of mechanical and thermal loads in pcBN tooling during machining of Inconel 718. *Int. J. Adv. Manuf. Technol.* **2020**, *107*, 1451–1462. [\[CrossRef\]](#)
9. Rahman, M.; Seah, W.K.H.; Teo, T.T. The machinability of Inconel 718. *J. Mater. Process. Technol.* **1997**, *63*, 199–204. [\[CrossRef\]](#)
10. Sousa, V.F.C.; Silva, F.J.G. Recent Advances on Coated Milling Tool Technology—A Comprehensive Review. *Coatings* **2020**, *10*, 235. [\[CrossRef\]](#)
11. Wojciechowski, S.; Przystacki, D.; Chwalczuk, T. The Evaluation of Surface Integrity During Machining of Inconel 718 with Various Laser Assistance Strategies. *MATEC Web Conf.* **2017**, *136*, 01006. [\[CrossRef\]](#)
12. Burghardt, A.; Szybicki, D.; Kurc, K.; Muszyńska, M.; Mucha, J. Experimental Study of Inconel 718 Surface Treatment by Edge Robotic Deburring with Force Control. *Strength Mater.* **2017**, *49*, 594–604. [\[CrossRef\]](#)
13. Sousa, V.F.C.; Da Silva, F.J.G.; Pinto, G.F.; Baptista, A.; Alexandre, R. Characteristics and Wear Mechanisms of TiAlN-Based Coatings for Machining Applications: A Comprehensive Review. *Metals* **2021**, *11*, 260. [\[CrossRef\]](#)
14. Fallbohmer, P.; Rodrigues, C.A.; Ozel, T.; Altan, T. High-speed machining of cast iron and alloy steels for die and mold manufacturing. *J. Mater. Process. Technol.* **2000**, *98*, 104–115. [\[CrossRef\]](#)
15. Liao, Y.; Lin, H. Mechanism of minimum quantity lubrication in high-speed milling of hardened steel. *Int. J. Mach. Tools Manuf.* **2007**, *47*, 1660–1666. [\[CrossRef\]](#)
16. Wang, B.; Liu, Z.Q.; Cai, Y.K.; Luo, X.C.; Ma, H.F.; Song, Q.H.; Xiong, Z.H. Advancements in material removal mechanism and surface integrity of high speed metal cutting: A review. *Int. J. Mach. Tools Manuf.* **2021**, *166*, 103744. [\[CrossRef\]](#)
17. Ezugwu, E.O. High speed machining of aero-engine alloys. *J. Braz. Soc. Mech. Sci. Eng.* **2004**, *26*, 1–11. [\[CrossRef\]](#)
18. Tu, L.Q.; Ming, W.W.; Xu, X.W.; Cai, C.Y.; Chen, J.; An, Q.L.; Xu, J.Y.; Chen, M. Wear and failure mechanisms of SiAlON ceramic tools during high-speed turning of nickel-based superalloys. *Wear* **2022**, *488–489*, 204171. [\[CrossRef\]](#)
19. Dudzinski, D.; Devillez, A.; Moufki, A.; Larrouquère, D.; Zerrouki, V.; Vigneau, J. A review of developments towards dry and high speed machining of Inconel 718 alloy. *Int. J. Mach. Tools Manuf.* **2004**, *44*, 439–456. [\[CrossRef\]](#)
20. Toenshoff, H.K.; Denkena, B. *Basics of Cutting and Abrasive Processes*; Springer: Berlin/Heidelberg, Germany, 2013. [\[CrossRef\]](#)
21. Criado, V.; Alvarez, J.D.; Cantero, J.L.; Miguélez, M.H. Study of the performance of PCBN and carbide tools in finishing machining of Inconel 718 with cutting fluid at conventional pressures. *Procedia CIRP* **2018**, *77*, 634–637. [\[CrossRef\]](#)
22. Giménez, S.; Van der Biest, O.; Vleugels, J. The role of chemical wear in machining iron based materials by PCD and PCBN super-hard tool materials. *Diam. Relat. Mater.* **2007**, *16*, 435–445. [\[CrossRef\]](#)
23. Zhangiang, L.; Xing, A. Cutting tool materials for high speed machining. *Prog. Nat. Sci.* **2005**, *15*, 777–783. [\[CrossRef\]](#)
24. Costes, J.; Guillet, Y.; Poulachon, G.; Dessoly, M. Tool-life and wear mechanisms of CBN tools in machining of Inconel 718. *Int. J. Mach. Tools Manuf.* **2007**, *47*, 1081–1087. [\[CrossRef\]](#)
25. Bushlya, V.; Zhou, J.; Avdovic, P.; Ståhl, J.-E. Performance and wear mechanisms of whisker-reinforced alumina, coated and uncoated PCBN tools when high-speed turning aged Inconel 718. *Int. J. Adv. Manuf. Technol.* **2013**, *66*, 2013–2021. [\[CrossRef\]](#)
26. Khan, S.; Soo, S.; Aspinwall, D.; Sage, C.; Harden, P.; Fleming, M.; White, A.; M'Saoubi, R. Tool wear/life evaluation when finish turning Inconel 718 using PCBN tooling. *Procedia CIRP* **2012**, *1*, 283–288. [\[CrossRef\]](#)
27. Soo, S.L.; Khan, S.A.; Aspinwall, D.K.; Harden, P.; Mantle, A.L.; Kappmeyer, G.; Pearson, D.; M'Saoubi, R. High speed turning of Inconel 718 using PVD-coated PCBN tools. *CIRP Ann.* **2016**, *65*, 89–92. [\[CrossRef\]](#)
28. Bushlya, V.; Zhou, J.; Ståhl, J. Effect of Cutting Conditions on Machinability of Superalloy Inconel 718 During High Speed Turning with Coated and Uncoated PCBN Tools. *Procedia CIRP* **2012**, *3*, 370–375. [\[CrossRef\]](#)
29. Bushlya, V.; Bjerke, A.; Turkevich, V.Z.; Lenrick, F.; Petrusha, I.A.; Cherednichenko, K.A.; Stahl, J.E. On chemical and diffusional interactions between PCBN and superalloy Inconel 718: Imitational experiments. *J. Europ. Ceramic Soc.* **2019**, *39*, 2658–2665. [\[CrossRef\]](#)

30. Sugihara, T.; Tanaka, H.; Enomoto, T. Development of Novel CBN Cutting Tool for High Speed Machining of Inconel 718 Focusing on Coolant Behaviors. *Procedia Manuf.* **2017**, *10*, 436–442. [\[CrossRef\]](#)
31. Sousa, V.F.C.; Silva, F.J.G. Recent Advances in Turning Processes Using Coated Tools—A Comprehensive Review. *Metals* **2020**, *10*, 170. [\[CrossRef\]](#)
32. Slama, C.; Servant, C.; Cizeron, G. Aging of Inconel 718 alloy between 500 and 750 °C. *J. Mater. Res.* **1997**, *12*, 2298–2316. [\[CrossRef\]](#)
33. Azarbarmas, M.; Aghaie-Khafri, M.; Cabrera, J.; Calvo, J. Dynamic recrystallization mechanisms and twinning evolution during hot deformation of Inconel 718. *Mater. Sci. Eng. A* **2016**, *678*, 137–152. [\[CrossRef\]](#)
34. Wu, Z.; Parish, C.; Bei, H. Nano-twin mediated plasticity in carbon-containing FeNiCoCrMn high entropy alloys. *J. Alloy. Compd.* **2015**, *647*, 815–822. [\[CrossRef\]](#)
35. Cantero, J.L.; Díaz-Álvarez, J.; Infante-García, D.; Rodríguez, M.; Criado, V. High Speed Finish Turning of Inconel 718 Using PCBN Tools under Dry Conditions. *Metals* **2018**, *8*, 192. [\[CrossRef\]](#)
36. Huang, Y.; Liang, S.Y. Modeling of Cutting Forces Under Hard Turning Conditions Considering Tool Wear Effect. *J. Manuf. Sci. Eng.* **2005**, *127*, 262–270. [\[CrossRef\]](#)
37. Bouacha, K.; Yallese, M.A.; Mabrouki, T.; Rigal, J.-F. Statistical analysis of surface roughness and cutting forces using response surface methodology in hard turning of AISI 52100 bearing steel with CBN tool. *Int. J. Refract. Met. Hard Mater.* **2010**, *28*, 349–361. [\[CrossRef\]](#)
38. Wanner, B.; Eynian, M.; Beno, T.; Pejryd, L. Process stability strategies in milling of thin-walled Inconel 718. *AIP Conf. Procc.* **2012**, *1431*, 465. [\[CrossRef\]](#)
39. Silva, T.E.; Amaral, A.; Couto, A.; Coelho, J.; Reis, A.; Rosa, P.A.; de Jesus, A.M. Comparison of the machinability of the 316L and 18Ni300 additively manufactured steels based on turning tests. *J. Mater. Des. Appl.* **2021**, *235*, 2207–2226. [\[CrossRef\]](#)
40. Bushlya, V.; Lenrick, F.; Bjerke, A.; Aboulfadl, H.; Thuvander, M.; Ståhl, J.-E.; M'Saoubi, R. Tool wear mechanisms of PcBN in machining Inconel 718: Analysis across multiple length scale. *CIRP Ann.* **2021**, *70*, 73–78. [\[CrossRef\]](#)
41. Bhattacharyya, S.K.; Jawaid, A.; Lewis, M.H.; Wallbank, J. Wear mechanisms of Sialon ceramic tools when machining nickel-based materials. *Metals Technol.* **1983**, *10*, 482–489. [\[CrossRef\]](#)
42. Xue, C.; Wang, D.; Zhang, J. Wear Mechanisms and Notch Formation of Whisker-Reinforced Alumina and Sialon Ceramic Tools during High-Speed Turning of Inconel 718. *Materials* **2022**, *15*, 3860. [\[CrossRef\]](#)
43. Tampieri, A.; Bellosi, A. Oxidation Resistance of Alumina-Titanium Nitride and Alumina-Titanium Carbide Composites. *J. Am. Ceram. Soc.* **1992**, *75*, 1688–1690. [\[CrossRef\]](#)

Disclaimer/Publisher's Note: The statements, opinions and data contained in all publications are solely those of the individual author(s) and contributor(s) and not of MDPI and/or the editor(s). MDPI and/or the editor(s) disclaim responsibility for any injury to people or property resulting from any ideas, methods, instructions or products referred to in the content.